Ligand-Induced Conformational Changes in Tissue Transglutaminase: Monte Carlo Analysis of Small-Angle Scattering Data

Paolo Mariani,* Flavio Carsughi,† Francesco Spinozzi,* Sandro Romanzetti,* Gerd Meier,‡ Rita Casadio,§ and Carlo M. Bergamini¶

*Istituto di Scienze Fisiche and Istituto Nazionale per la Fisica della Materia, Università, I-60131 Ancona, Italy; †Facoltà di Agraria and Istituto Nazionale per la Fisica della Materia, Università, I-60131 Ancona, Italy; ‡MPI-Polymerforschung, D-55021 Mainz, Germany; §Dipartimento di Biologia, Università di Bologna, I-40100 Bologna, Italy; and ¶Dipartimento di Biochimica e Biologia Molecolare, Università di Ferrara, I-44100 Ferrara, Italy

ABSTRACT Small-angle neutron and x-ray scattering experiments have been performed on type 2 tissular transglutaminase to characterize the conformational changes that bring about Ca^{2+} activation and guanosine triphosphate (GTP) inhibition. The native and a proteolyzed form of the enzyme, in the presence and in the absence of the two effectors, were considered. To describe the shape of transglutaminase in the different conformations, a Monte Carlo method for calculating small-angle neutron scattering profiles was developed by taking into account the computer-designed structure of the native transglutaminase, the results of the Guinier analysis, and the essential role played by the solvent-exposed peptide loop for the conformational changes of the protein after activation. Although the range of the neutron scattering data is rather limited, by using the Monte Carlo analysis, and because the structure of the native protein is available, the distribution of the protein conformations after ligand interaction was obtained. Calcium activation promotes a rotation of the C-terminal with respect to the N-terminal domain around the solvent-exposed peptide loop that connects the two regions. The ψ angle between the longest axes of the two pairs of domains is found to be above 50°, larger than the ψ value of 35° calculated for the native transglutaminase. On the other hand, the addition of GTP makes possible conformations characterized by ψ angles lower than 34°. These results are in good agreement with the proposed enzyme activity regulation: in the presence of GTP, the catalytic site is shielded by the more compact protein structure, while the conformational changes induced by Ca^{2+} make the active site accessible to the substrate.

INTRODUCTION

Tissular transglutaminases (TG-ases) are monomeric proteins with a molecular mass of ~80 kDa that act as bifunctional enzymes to catalyze either the posttranslational modification of proteins at glutamine residues, with formation of isopeptide bonds (Greenberg et al., 1991; Folk and Fynnlayson, 1977), or the transduction of extracellular hormonal signals, behaving like G-like proteins (Nakaoka et al., 1994; Monsonego et al., 1998). Apparently, this dual role is carried out by distinct conformations of the protein, stabilized by the interaction with the ligands Ca^{2+} and guanosine triphosphate (GTP), in relation to different cellular physiological processes, such as the onset of the cell death program (Fesus et al., 1991) or the progression of the cell cycle (Mian et al., 1995). At the normal physiological concentration of calcium (the essential activator) and GTP (an allosteric inhibitor), the enzyme is kept inactive; under conditions where the Ca^{2+} concentration is raised and the cell GTP declines, as in irreversibly damaged cells, the enzyme becomes active and leads to cell death, as in terminal differentiation in keratinocytes and apoptosis (Bergamini and Signorini, 1993; Smethurst and Griffin, 1996; Zhang et al., 1998).

The crystallographic structure of TG-ase is not known, but much has been learned about possible structural changes in the secondary and tertiary structures of transglutaminases under the influence of ligands (Tanfani et al., 1993). In particular, Ca^{2+} binds to relatively high-affinity binding sites (up to six), activating the enzyme through conformational changes that allow exposure of the active site to the incoming protein substrate (Bergamini, 1988). In contrast, GTP binds to a single site, hampering Ca^{2+} binding and related structural modifications. Recently, a computer-designed model for the structure of the tissue type 2 TG-ase, based on the sequence homology with human factor XIIIa, has been proposed and validated by means of small-angle neutron scattering (Casadio et al., 1999). The data indicate that the protein can be approximated by a prolate ellipsoidal shape with axis lengths of 62, 42, and 110 Å and is composed of four domains, assembled in two pairs that can be separated into N- and C-terminal regions by limited proteolysis. The active site is buried in a cleft between the two regions, hidden from the contact with the solvent or with the macromolecular substrates. The model presents an interesting feature: 50-ps protein dynamics studies show that the two protein regions move apart with the addition of Ca^{2+}, thus disclosing the active site for catalysis (Casadio et al., 1999). These observations suggested that conformational changes induced by calcium regulate the enzyme activity. Small-angle scattering of x-rays (SAXS) or neutrons

Received for publication 17 May 1999 and in final form 25 February 2000.

Address reprint requests to Dr. Paolo Mariani, Istituto di Scienze Fisiche, Facoltà di Medicina e Chirurgia, Università di Ancona, Via Ranieri 65, I-60131 Ancona, Italy. Tel.: 39-071-2204608; Fax: 39-071-2204605; E-mail: p.mariani@alisf1.unian.it.

0006-3495/00/06/3240/12 $2.00

(SANS) is one of the most suitable approaches to the study of biopolymer structure in solution (Jacrot, 1976; Glatter and Kratky, 1982; Chen and Bendedouch, 1986; Kataoka et al., 1995; Svergun and Stuhrman, 1991; Svergun et al., 1998). In particular, because of the dependence on the geometric shape, small-angle scattering data can be sensitive to domain orientations and dispositions and hence to conformational changes, which can be the key to understanding biomolecular mechanisms (Trewhella, 1997). However, because of the low resolution and the loss of information incurred from averaging the scattered intensity over all particle orientations in the usual case of scattering from isotropic solution, the derivation of the particle structure from the experimental SAS curve is a rather tough problem, the solution of which might not be unique. To reconstruct the shape of the scattering particles, different procedures have been used, some of which are direct (such as the well-established method based on the multipole expansion of the excess scattering length density; Svergun and Stuhrman, 1991; Svergun, 1991; Spinozzi et al., 1998), while others usually require the comparison of the form factor of a model shape (or from a mixture of known structures) to the experimentally observed scattering function. The structures to be compared can be simple geometrical models (Guinier and Fournet, 1955), complex heterogeneous particles built from any number and orientation of simple building blocks or can be directly evaluated from the crystallographic coordinates. The procedure adopted for model refinement ranges from the usual trial-and-error approaches to Monte Carlo or genetic algorithms (see, for example, Hansen, 1990; Mayans et al., 1995; Henderson, 1996; Ashton et al., 1997; Svergun, 1997; Chacon et al., 1998, and references therein). Recently, the comparison between SANS and SAXS scattering curves and those evaluated from crystallographic structures also demonstrated the essential role of the protein hydration shell, the scattering density of which may differ by 5–25% from that of the bulk (Svergun et al., 1998).

In the present paper, SANS and SAXS experiments performed on TG-ase in solution are described and analyzed using a Monte Carlo simulation technique to obtain molecular details of the conformational changes. In particular, the enzyme was analyzed in the native and in a proteolyzed form, both in the presence and in the absence of the two effectors. The full analysis of small-angle scattering data demonstrates that after Ca^{2+} activation, large conformational changes are brought about by rotating the N-terminal region with respect to the C-terminal region around a solvent-exposed peptide loop. The Monte Carlo procedure shows that the angle between the longest axes of the two regions, which in the native protein is 34.6°, should be at least 50°. On the other hand, the presence of GTP allows the N- and C-terminal regions to be even closer. Moreover, SAS data show that selective cleavage by proteinases of the peptide chain at a loop connecting the N- and C-terminal regions prevents the protein widening due to Ca^{2+}, confirming the essential role of the flexible loop in the protein structural changes after activation.

MATERIALS AND METHODS

Sample preparation

The purification of erythrocyte native type 2 tissular TG-ase (nTG-ase) proceeded through chromatography on diethylaminoethyl (DEAE) cellulose, DEAE-Sepharose, fractionation with polyethylene glycol, and affinity chromatography on immobilized heparin. Sodium dodecyl sulfate-polyacrylamide gel electrophoresis (SDS-PAGE) indicated that TG-ase was homogeneous, although nonenzymatic fragmentation was taking place during storage, as previously described (Bergamini and Signorini, 1993).

Proteolyzed samples (pTG-ase), in which the TG-ase chain is cleaved at the flexible loop to generate two peptides with apparent molecular masses of 56 kDa and 31 kDa, as determined by SDS-PAGE, were obtained as previously described (Casadio et al., 1999). TG-ase was incubated with chymotrypsin at a 1.25% weight ratio in 50 mM Tris, 1 mM mercaptoethanol (pH 7.5), for ~90 min, with, if required, the addition of 2 mM $CaCl_2$ or 0.5 mM GTP. Proteolysis was blocked by the addition of phenylmethylsulfonyl fluoride. The mixture was analyzed for residual activity and extent of proteolysis by a standard amine incorporation assay into dimethylcasein and by SDS-PAGE, and a quantitative determination of the remaining intact protein was made by densitometry of the stained gel (Casadio et al., 1999). Completely digested proteins were employed for SAS analysis.

For SANS measurements, both native and proteolyzed TG-ase samples were dissolved in 20 mM Tris, 50 mM NaCl, 0.5 mM mercaptoethanol, 0.1 mM EDTA buffer (pH 7.5) prepared with deuterated water. The final protein concentration was adjusted to 5 and 2.5 mg/ml. Three different series of samples were investigated: in the first, native TG-ase was analyzed pure and after the addition of 2.5 mM $CaCl_2$, of 0.5 mM GTP, and of 2.5 mM $CaCl_2$ and 0.5 mM GTP, respectively. In the second series, the proteolyzed enzyme was analyzed under the conditions reported above. In the last series, 0.5, 2.6, and 4 M guanidine-HCl (Gdn-HCl) were respectively added to the proteolyzed enzyme. For SAXS measurements, TG-ase samples were dissolved in the same pH 7.5 buffer, prepared in light water at a nominal concentration of 2.5 mg/ml. The analyzed samples were nTG-ase, pTG-ase, and pTG-ase in 0.5, 0.8, 1.0, and 2.0 M Gdn-HCl.

Protein model

The type 2 tissular TG-ase is a monomeric protein with a molecular mass of 77,125 Da, as calculated from the amino acid composition (Nakanishi et al., 1991). The protein volume, which excludes the solvent, V, and the total coherent scattering length Σb, which are implied in SANS data analysis (see below), were also derived from the amino acid composition, using volumes and scattering lengths of the amino acid residues reported by Jacrot and Zaccai (Jacrot, 1976; Jacrot and Zaccai, 1981). The resulting volume V is ~97,000 $Å^3$, and the total coherent scattering length $\Sigma b = 3.0 \times 10^{-9}$ cm.

The computer-designed model for the structure of the native TG-ase, recently reported by our group (Casadio et al., 1999), is shown in Fig. 1 (views *a* and *b*). Four domains have been identified: the N-terminal domain (no. 1, *orange*) contains 139 amino acids and is characterized by large contributions of β structures; the second domain (no. 2, *yellow*) extends from amino acid 140 to amino acid 454 and contains all α helical regions of the protein. In this domain are situated the three putative Ca^{2+}-binding regions and the active site (Nakanishi et al., 1991; Pedersen et al., 1994). The active center (comprising Cys^{277}, His^{335}, and Asp^{358}, in *red*) is buried within a narrow cleft, the walls of which are formed by the domain itself and by the two C-terminal domains no. 3 (*cyan*) and no. 4 (*blue*). These two

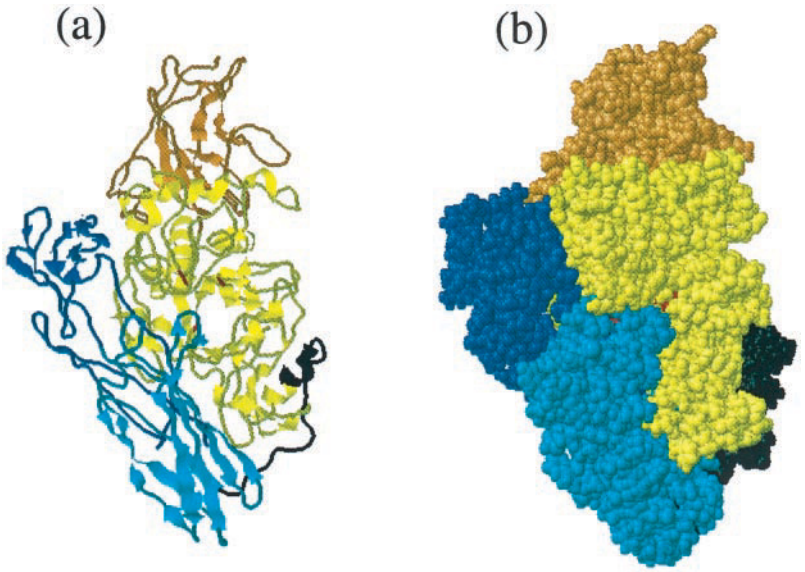

FIGURE 1 Three-dimensional representations of the structure of tissue-type TG-ase, using the RasMol 2.6 package (www.umass.edu/microbio/rasmol/). The four domains assembled into two peptides p56 and p31 of the enzyme are shown in different colors. The N-terminal p56 peptide includes the domains 1 (*orange*) and 2 (*yellow*), and the C-terminal p31 peptide includes domains 3 (*cyan*) and 4 (*blue*). The active site, hidden in a narrow cleft between these two regions, is shown in red. The exposed loop, which is the preferred site of cleavage by proteinases and connects domains 2 and 3, is shown in black. (*a*) Computer-designed model of the structure of TG-ase, redrawn from Bergamini et al. (1998). View using "cartoon" option of RasMol 2.6. (*b*) As in *a*, with "spacefill" option.

domains (from 479–585 and 586–687 amino acid residues, respectively) are largely represented by β structures arranged in a barrel-like conformation. The connection between domains 2 and 3 is a flexible solvent-exposed loop of 24 amino acids (*black*). The overall shape of the protein approximates a wide prolate semiellipsoid with a flat basis, with axes of 64, 44, and 110 Å. The theoretical radius of gyration, $R_{g,th}$, calculated as indicated below from the atomic coordinates, is 29.6 Å.

When the TG-ase is subjected to limited proteolysis, two peptides of 56 kDa and 31 kDa are generated (Casadio et al., 1999). The enzyme chain is cleaved in the exposed loop between the 455 and 478 amino acids: according to the structure model, the 56-kDa peptide (labeled p56) corresponds to the N-terminal domains 1 and 2, and the 31-kDa peptide (p31) to the C-terminal domains 3 and 4. Theoretical radii of gyration of $R_{g,p56}$ = 26.0 Å and $R_{g,p31}$ = 23.6 Å were calculated using the atomic coordinates of the two peptides directly obtained from the computer-designed model.

Small-angle neutron and x-ray scattering experiments

Small-angle neutron scattering (SANS) experiments were performed at room temperature, using two different instruments, namely the V4 diffractometer of the Hahn-Meitner Institut (HMI) in Berlin (D) and the KWS II diffractometer of the ForschungsZentrum Julich (FZJ) in Julich (D). At HMI, the scattering vector Q ranges ($Q = 4\pi \sin\theta/\lambda$, where 2θ is the scattering angle, λ is the neutron wavelength) from 0.026 to 0.054 $Å^{-1}$ for the nTG-ase and nTG-ase/GTP samples and from 0.026 to 0.078 $Å^{-1}$ in the case of nTG-ase/Ca^{2+}. At FZJ, the Q range for all samples was 0.012 ÷ 0.078 $Å^{-1}$.

TG-ase samples were measured in 2-mm quartz cells. SANS profiles were usually obtained in ~6 h, with less than 5% statistical error for the smallest angle. The experimental intensities were corrected for background and buffer contributions, for detector inhomogeneities, and for sample transmission. The scattering cross sections have been converted to absolute units ($d\Sigma/d\Omega$, in cm^{-1}) by calibration with 1 mm of light water (HMI) and 2 mm of polyethylene (FZJ).

SAXS measurements were performed by using a SAS pinhole camera, installed on a Rigaku-Denki (Japan) rotating anode working at 8 kW. The wavelength of x-rays was 1.54 Å. The investigated Q range is 0.017–0.25 $Å^{-1}$. In this case, protein solutions were measured in 2-mm quartz capillaries (Hilgenberg, Malsfeld, D). The experimental intensities were corrected for background and buffer scattering and for sample transmission. Only relative scattering intensities were obtained.

SAS data analysis

The neutron (x-ray) scattering cross section from a system of N identical heterogeneous particles per unit volume, composed of n_D different domains with a constant scattering density (coherent scattering length or electron density in SANS and SAXS, respectively) ρ_i and volume V_i and embedded in a homogeneous solvent of scattering density ρ_S, widely separated and with a fully isotropic orientation, can be written as

$$\frac{d\Sigma}{d\Omega}(Q) = N(\Delta\rho)^2 V^2 P(Q), \tag{1}$$

where $V = \sum_{i=1}^{n_D} V_i$ is the scattering particle volume, $\Delta\rho$ is the contrast, defined in terms of volume fractions $\varphi_i = V_i/V$ of phase i,

$$\Delta\rho = \left[\sum_{i=1}^{n_D} \rho_i \varphi_i\right] - \rho_S, \tag{2}$$

and $P(Q)$ is the squared form factor (orientationally averaged), which depends on the size, shape, scattering density ρ_i, and volume fraction φ_i of the n_D particle domains (Guinier and Fournet, 1955).

At small Q, the form factor $P(Q)$ can be approximated by the so-called Guinier law,

$$P(Q) \approx \exp(-R_g^2 Q^2/3), \tag{3}$$

where R_g is the gyration radius, which for a multidomain particle can be expressed as a combination of partial radii R_{ij} by

$$R_g^2 = \frac{1}{(\Delta\rho)^2} \sum_{i,j=1}^{n_D} (\rho_i - \rho_S)(\rho_j - \rho_S)\varphi_i\varphi_j R_{ij}^2, \tag{4}$$

$$R_{ij}^2 = \frac{1}{2}\int_0^\infty dr\, r^2 p_{ij}(r), \tag{5}$$

where $p_{ij}(r)$ represents the probability that a vector of length r has one end in the phase i and the other end in the phase j. Because $P(0) = 1$, the cross section at zero angle is given by

$$\frac{d\Sigma}{d\Omega}(0) = N(\Delta\rho)^2V^2. \quad (6)$$

Because of the impossibility of discriminating the SAS signal from the primary beam at low Q and from the background at large Q, a measurement can only investigate a finite Q range. If the Guinier law is satisfied, the gyration radius R_g and the $d\Sigma/d\Omega(0)$ value can be obtained by a linear fit of the experimental data in the so-called Guinier plot, i.e., $\ln[d\Sigma/d\Omega(Q)]$ versus Q^2.

In the case of heterogeneous particles, the presence of domains of different scattering density results in the variation of R_g and $d\Sigma/d\Omega(0)$ with the contrast $\Delta\rho$ (Jacrot, 1976). Because of the contrast dependence, information about the role of the protein hydration in solution can be also obtained (Svergun et al., 1998): for some proteins, the density of the water (and then its scattering density) in the border layer has been proved to be higher than the density of the bulk water. Therefore, the solution scattering pattern from a given crystal structure is proportional to the scattering from the single particle (evaluated from the atomic coordinates), but the scattering from the excluded volume (filled with bulk solvent with constant scattering density) and from the hydration shell should also be taken into account. Nevertheless, the mobility of the chains on the protein surface can determine a change in the scattering density profile at the protein-solvent interface (Svergun et al., 1998).

A simple way to establish the structure of the particle border is the comparison of gyration radii obtained from X-ray scattering and from neutron scattering experiments performed in D_2O and in H_2O (Ashton et al., 1997; Svergun et al., 1998). In particular, when the experimental radii of gyration are similar (and then they appear to be independent on the contrast; see Eq. 4 for $n_D = 1$), the presence of a hydration shell around the protein that is denser than the bulk solvent can be excluded, and both SANS and SAXS data can be analyzed, assuming a homogeneous scattering density for the protein (Guinier and Fournet, 1955; Jacrot, 1976). As we will show below, this is the situation that occurs in the present case, and only the mobility at the interface will be taken into account.

In the case of homogeneous particles, the distance distribution function $p(r)$, which represents the frequency of vectors of modulus r connecting small volume elements within the entire volume of the scattering particle, can be expressed as the isotropic Fourier transform of the scattering function (Guinier and Fournet, 1955),

$$p(r) = \frac{2r}{\pi}\int_0^\infty P(Q)Q\sin(Qr)dQ. \quad (7)$$

The convergence of this transform depends on the maximum value Q_{max} of the experimental curve $d\Sigma/d\Omega(Q)$. When the (crystallographic) structure of the particle is known, the $p(r)$ function can be calculated and then, by inverse Fourier transform of Eq. 7,

$$P(Q) = \int_0^\infty p(r)\frac{\sin(Qr)}{Qr}dr, \quad (8)$$

the scattering profile is reproduced. The comparison between the experimental and the reproduced SAS curves is a straightforward method for detecting changes in protein secondary, tertiary, or quaternary structure eventually occurring in solution.

In this paper, following the procedure described by Hansen (1990), a Monte Carlo simulation of the scattering volume is used to directly calculate from the crystallographic coordinates the distance distribution function $p(r)$ and then the SAS profile. To reproduce the experimental curves observed in the presence of ligands, a protein model fitting procedure has also been developed. In detail, the homogeneous scattering particle (in terms of shape and size) has been described by the function $s(\mathbf{r})$, which gives the probability that the point $\mathbf{r} \equiv (r, \omega_r)$ (where ω_r indicates the polar angles α_r and β_r) lies within the particle. For compact particles like globular proteins, this function can be written in terms of a unique two-dimensional angular shape function $\mathcal{F}(\omega_r)$ as

$$s(\mathbf{r}) = \begin{cases} 1 & r \le \mathcal{F}(\omega_r) \\ \exp\{-[r - \mathcal{F}(\omega_r)]^2/2\sigma^2\} & r > \mathcal{F}(\omega_r), \end{cases} \quad (9)$$

where σ is the width of the Gaussian that accounts for the particle surface mobility (Svergun, 1997; see also Svergun et al., 1998, for more complex cases). Once the protein model is known, the shape function $\mathcal{F}(\omega_r)$ is evaluated from the envelope surface of the van der Waals spheres centered in each atom. By fixing the axis origin on the mean value of the atomic coordinates, the $\mathcal{F}(\omega_r)$ is determined, running over each atom j and taking the maximum distance r between the origin and the intersection, if any, of the van der Waals sphere centered in j with the direction ω_r. Assuming homogeneous particles, M random points are generated from polar coordinates. The sampling is made for the variables α_r, $\cos\beta_r$, and r^3 in the ranges $[0, 2\pi]$, $[-1, 1]$ and $[0, r^3_{max}]$, respectively. Following Eq. 9, if $r_j \le \mathcal{F}(\omega_{r_j})$, the point j is accepted, otherwise the probability $p = \exp\{-[r_j - \mathcal{F}(\omega_{r_j})]^2/2\sigma^2\}$ is calculated. A random number y between 0 and 1 is extracted, and if $y < p$, the point j is accepted and otherwise is rejected. The $p(r)$ histogram of the particle is then calculated by taking into account the distances between all possible pairs of M points,

$$p(r) = \frac{2}{\Delta r M(M-1)}\sum_{i=1}^{M-1}\sum_{j=i+1}^{M} H(\Delta r/2 - |r - r_{ij}|), \quad (10)$$

where Δr is the grid amplitude in the space of radial distance and r_{ij} is the distance between the points i and j. $H(x)$ is a step function ($H(x) = 0$ if $x < 0$ and $H(x) = 1$ if $x \ge 0$).

This method has been extended to describe the scattering volume of particles constituted by several subunits. Each subunit k, described by the function $\mathcal{F}_k(\omega_r)$, is oriented by Ω_k with respect to a reference frame and placed in the position $\mathbf{R}_k$. It is important to point out that to generate uniform scattering density in the whole particle, the number of random points for each subunit k should be proportional to its volume (subvolume). This can be achieved by considering M_A random attempts within a unique sphere of radius r_{max}, the center of which is used as the center of each subvolume. In the present case, we used $M_A = 10^6$ and $r_{max} = 170$ Å. All points in each subvolume k are then translated and rotated to construct the whole scattering volume. The common portions of space between two or more subunits are checked with the method developed by Hansen (1990).

The same procedure has also been used to describe conformational changes in the protein. According to the TG-ase model discussed below, we considered the case of a scattering particle constituted by two subunits that can rotate around a hinge. The two angular shape functions $\mathcal{F}_1(\omega_r)$ and $\mathcal{F}_2(\omega_r)$ describing the two subunits can be evaluated from the atomic coordinates. Let $\mathbf{R}^h_1$ and $\mathbf{R}^h_2$ be the hinge atom vector positions in the two reference frames: each possible particle configuration is then obtained by rotating the second subunit with respect to the first by three Euler angles Ω_2, calculating the new position of the hinge atom $\mathbf{R}^h_2(\Omega_2)$, and translating all atoms of the second unit in the position $\mathbf{R}^h_1 - \mathbf{R}^h_2(\Omega_2)$ (see Fig. 2).

The analysis of the experimental curves $d\Sigma/d\Omega(Q)$ of N_Q points has been performed by minimizing the reduced chi squared,

$$\chi^2 = \frac{1}{N_Q - N_P}\sum_{i=1}^{N_Q}\left[\frac{d\Sigma/d\Omega(Q_i) - \kappa P(Q_i) - B}{\delta_i}\right]^2, \quad (11)$$

where $P(Q)$ is determined from Eq. 8; κ and B are a scaling factor, related to the constants in Eq. 6, and a flat background, due to the incoherent

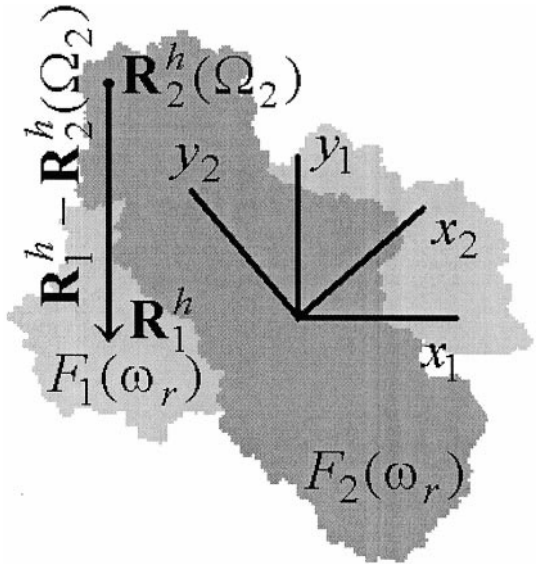

FIGURE 2 Sketch of the two angular shape functions $\mathcal{F}_1(\omega_r)$ (*light gray*) and $\mathcal{F}_2(\omega_r)$ (*dark gray*), which describe the two particle subunits. $\mathbf{R}_1^h$ and $\mathbf{R}_2^h$ are the positions of the hinge atom in the two reference frames (x_1, y_1, z_1) and (x_2, y_2, z_2), respectively. The final particle configuration is obtained by rotating $\mathcal{F}_2(\omega_r)$ by three Euler angles Ω_2, calculating the new position of the hinge atom $\mathbf{R}_2^h(\Omega_2)$, and translating the second unit in the position $\mathbf{R}_1^h - \mathbf{R}_2^h(\Omega_2)$.

scattering, respectively; δ_i is the experimental uncertainty of the scattering curve at the point Q_i. N_P is the number of fitting parameters, which, in the present case, are the Gaussian width σ and the Euler angles Ω_2. Corrections were applied for neutron wavelength band or beam divergence, as described by Ashton and co-workers (1997).

RESULTS

Structural properties of the native TG-ase and ligand effects

Experimental SANS profiles obtained at HMI from samples of native TG-ase dissolved in D_2O buffer with and without GTP or Ca^{2+} are reported in Fig. 3. The corresponding Guinier plots are shown in Fig. 4, together with other SANS profiles obtained under different experimental conditions. Nearly identical curves were obtained for TG-ase in the absence of ligands and in the presence of saturating amounts of GTP, while significant differences were observed for the enzyme incubated in the presence of 2.5 mM $CaCl_2$ and in the presence of both ligands, each added at its own saturating concentration. Gyration radii and $d\Sigma/d\Omega(0)$ values were derived using Eq. 3; the results are listed in Table 1. In particular, while GTP (the inhibitor) reduces the R_g of the nTG-ase only slightly, Ca^{2+} (the activator) increases it from 31 to ~38 Å. However, in nTG-ase containing both Ca^{2+} and GTP, the effect of the activator appears predominant, because the measured radius of gyration matched closely the one measured in the presence of Ca^{2+} alone. This result completely agrees with a previous report of kinetic studies (Bergamini, 1988), in which the combined actions of Ca^{2+} and GTP on the enzyme activity were considered.

Within the experimental errors, the radii of gyration measured by neutron scattering at the two investigated concentrations were found to be similar (see Table 1), indicating that interaction effects can be disregarded, i.e., the observed radii of gyration can be equated to the actual enzyme molecular parameter. Similar results were also obtained from SAXS measurements performed on TG-ase in light water (Table 2), suggesting that the radius of gyration is independent of the contrast. The comparative analysis of the radii of gyration obtained from SANS and SAXS data ($R_g \approx$ 31.5 Å) and those evaluated from the computer-designed structure of TG-ase ($R_{g,th}$ = 29.6 Å) provides an indication of an increase in the apparent protein size in solution. According to previous results (Svergun et al., 1998), such an increase should be attributed to the mobility or disorder of the side chains on the protein surface, due to solvent penetration.

From the forward neutron scattering, $d\Sigma/d\Omega(0)$, the concentrations of scattering particles in solution N were derived using Eq. 6. The results are reported in Table 1: the comparison with the nominal protein concentrations indicates that the native TG-ase is in a monomeric state, with and without the ligands. On the other hand, it was found by analytical ultracentrifugation that only limited changes were detected in the sedimentation coefficient of native protein alone or supplemented with Ca^{2+} or GTP (Bergamini, 1988; Casadio et al., 1999). Therefore, the modification of the radius of gyration measured by SANS in the presence of Ca^{2+} cannot be ascribed to significant reversible (dimerization) or irreversible (formation of isopeptide bonds) protein aggregation. Data support the view that we are indeed dealing with conformational changes that are strictly related to enzyme regulation.

Structural properties and ligand effects on the proteolyzed enzyme

As reported before, the proteolysis cleaves the protein at a single peptide bond in the exposed loop, connecting the two peptides p56 and p31. The cleaved enzyme was analyzed by SAS in the absence of ligands and in the presence of Ca^{2+}. Guanidine effects were also considered. It should be observed that in all of the proteolyzed samples, small amounts of precipitated material were recovered from the measurement cells, indicating a strong aggregation after proteolysis, as previously reported for other proteins (Jacrot and Zaccai, 1981; Chen and Bendedouch, 1986). In the present case, biochemical evidence suggests that the aggregation should depend on strong interactions between the N-terminal domains (C. M. Bergamini, unpublished observations).

Experimental SANS and SAXS profiles are reported in the form of Guinier plots in Figs. 5 and 6. All of the curves clearly show a linear behavior, even if the sharp upward

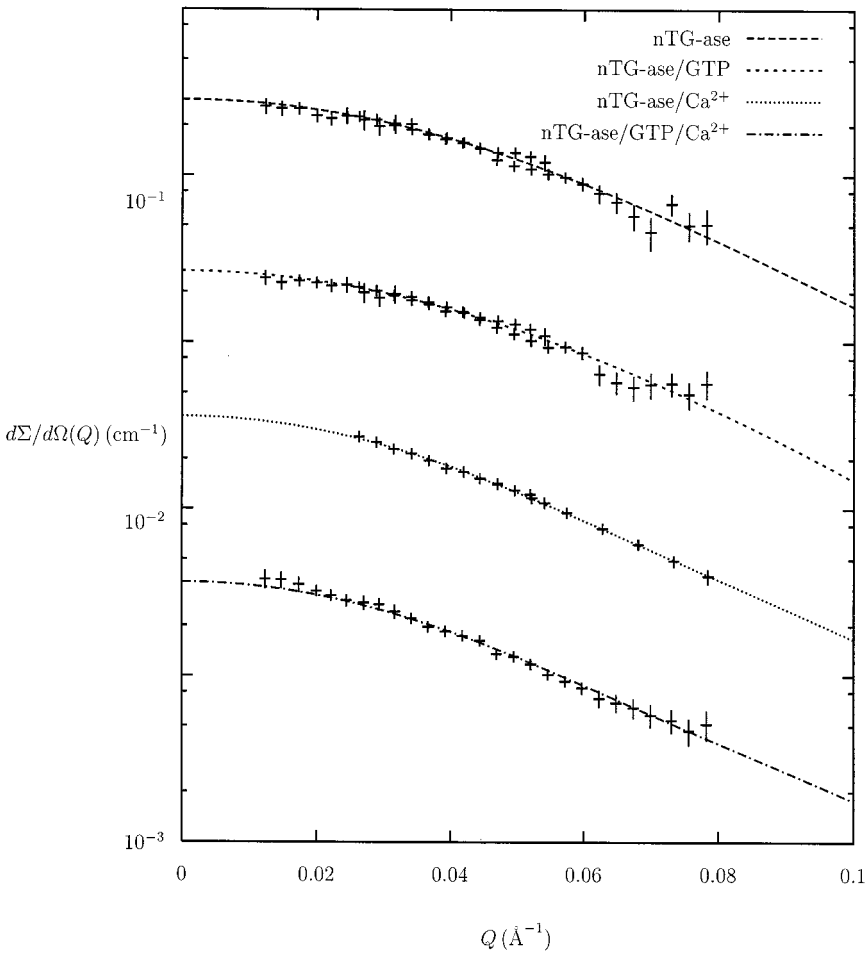

FIGURE 3 SANS profiles obtained at HMI and FZJ for the TG-ase dissolved in D_2O buffer in different experimental conditions. The curves are scaled for clarity. From the top: nTG-ase without ligands, with 0.4 mM GTP (scaled by 10^{-1}), with 1.8 mM $CaCl_2$ (scaled by 10^{-2}), with 0.4 mM GTP and 1.8 mM $CaCl_2$ (scaled by 10^{-3}). The solid lines correspond to fits SANS calculated by using the Monte Carlo method described in the text. The parameters obtained from the analysis are shown in Table 3.

deviation of the points at the very small angle region (see, in particular, neutron scattering curves) seems to reflect the presence of macroaggregates. However, it has been shown that the effect of very large aggregates in the system is negligible in the Guinier analysis at relatively large angles that more closely correspond to the real Guinier features of the protein (Guinier and Fournet, 1955; Eliezer et al., 1993; Shi et al., 1996). $d\Sigma/d\Omega(0)$ and R_g values have then been determined, considering the linear scattering region at larger angles on the Guinier plots (see Fig. 5). The results are listed in Tables 1 and 2. Some aspects are noticeable: first, the radius of gyration of the proteolyzed enzyme is close (inside the experimental error) to the one observed for the native TG-ase, indicating that after proteolysis the two N- and the C-terminal protein fragments are still joined, probably by hydrogen and electrostatic bonds. Second, within the experimental error, the radius of gyration is not affected by GTP or by the presence of Ca^{2+}, demonstrating that the cleavage of the peptide chain at the exposed loop prevents the occurrence of any conformational change. Third, SANS and SAXS results coincide, indicating that solute-solvent contrast effects were negligible in this case.

The analysis of the forward neutron scattering, $d\Sigma/d\Omega(0)$ (see Table 1), confirms the extensive aggregation of the proteolyzed enzyme and/or single peptides: the values of protein concentrations obtained experimentally are much lower than the nominal ones.

To identify the presence of smaller particles, namely the two disjoined p56 and p31 peptides, and estimate their size, SAS analysis of the proteolyzed enzyme has then been performed in the presence of an increasing concentration of guanidine (from 0.5 to 4 M). Guanidine is in fact expected to interfere with hydrogen and electrostatic bonds, lying at the interface between the two peptides. Accordingly, SAS results are very sensitive to guanidine concentration: 0.5 M guanidine does not break interpeptide bonds (see the SANS curve in Fig. 5), while, at the higher concentration, the absence of any scattering signal in the investigated Q range indicates that the protein is denatured. At intermediate guanidine concentrations (see Fig. 6, where the SAXS curves obtained at 0.8 and 1 M guanidine are reported), the data are consistent with the presence of particles with a gyration radius of ~19 Å. However, no other linear regions were detected in the Guinier plot reported in Fig. 6, hence

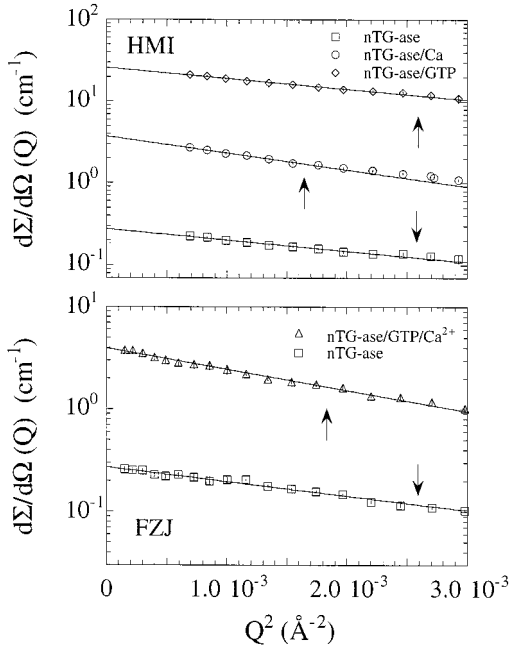

FIGURE 4 Guinier plots of SANS data measured at HMI (*top*) and at FZJ (*bottom*) for the native TG-ase dissolved in D_2O buffer without ligands (□), with 1.8 mM $CaCl_2$ (○, scaled by 10), with 0.4 mM GTP (◇, scaled by 10^2), and with 1.8 mM $CaCl_2$ and 0.4 mM GTP (△, scaled by 10). The solid lines correspond to the fit using the Guinier law. The maximum Q^2 values used for the fits are indicated by arrows.

excluding the presence of another family of scattering particles.

Size and shape analysis: the conformational changes in nTG-ase

The size and shape of native TG-ase samples were first analyzed in terms of their gyration radii. According to Guinier and Fournet (1955) and Chen and Bendedouch (1986), in fact, the value of R_g can be explicitly given in terms of the geometrical parameters of the particle. The radius of gyration of an ellipsoid of revolution with semi-axes a, b, and c is $[(a^2 + b^2 + c^2)/5]^{1/2}$. Using the radii of gyration obtained experimentally and the protein volume, the axis lengths have then been calculated assuming a circular section of the ellipsoidal model (i.e., $a = b$). For the native protein, the resulting long axis $2c$ is ~129 Å, while the shorter axes are ~37 Å. As previously observed, these values agree quite well with the dimensions of the computer-generated model (Casadio et al., 1999).

In the same simple way, shape information was obtained for the proteolyzed enzyme. Within the experimental error, the 19.0 ± 5.6 Å gyration radius observed in SAXS experiments roughly corresponds to the theoretical radius of gyration of the C-terminal peptide p31 ($R_{g,p31}$ = 23.6 Å, as calculated using the corresponding atomic coordinates obtained from the computer-designed model). Therefore, we suggest that in these conditions the N-terminal larger peptide p56 is fully denatured, in agreement with very recent measurements of the unfolding behavior of TG-ase (C. M. Bergamini, unpublished observations). Two transitions at 50° and 60° were in fact detected by microcalorimetry, and, by analysis of the triptophane fluorescence, the first one was assigned to the thermal denaturation of the p56 peptide. However, other explanations are also possible: the size of the peptides in solution could be reduced compared with the atomic structure because structural changes occur after complete separation of the two peptides.

To obtain information on the size and shape of TG-ase in the presence of ligands, we analyzed the SANS profile, using the Monte Carlo method described above. However, because of the low quality of the x-ray data, only neutron scattering measurements were considered for the particle shape reconstruction. In particular, where possible, HMI and FZJ data were combined by a proper intercalibration. For the TG-ase samples in the presence of Ca^{2+} and in the

TABLE 1 SANS experimental results

	R_g (Å)	dΣ/dΩ(0) (cm^{-1})	N (10^{16} cm^{-3})	% diff.	Instrument
nTG-ase	31.4 ± 0.5	0.279 ± 0.004	2.77 ± 0.04	28	HMI
nTG-ase	31.9 ± 1.4	0.108 ± 0.008	1.07 ± 0.08	27	FZJ
nTG-ase/Ca^{2+}	38.3 ± 1.3	0.375 ± 0.013	3.71 ± 0.13	5	HMI
nTG-ase/GTP	29.6 ± 0.5	0.259 ± 0.004	2.56 ± 0.04	7	HMI
nTG-ase/GTP	29.9 ± 0.7	0.140 ± 0.010	1.36 ± 0.10	7	FZJ
nTG-ase/GTP/Ca^{2+}	38.0 ± 0.8	0.192 ± 0.006	1.90 ± 0.06	−26	FZJ
pTG-ase	29.8 ± 2.6	0.029 ± 0.019	0.25 ± 0.16	80	FZJ
pTG-ase/Ca^{2+}	30.7 ± 3.8	0.021 ± 0.011	0.21 ± 0.11	87	FZJ
pTG-ase/Gdn-HCl 0.5 M	29.8 ± 3.1	0.013 ± 0.002	0.14 ± 0.02	93	FZJ
pTG-ase/Gdn-HCl 2.6 M	—	—	—	—	FZJ
pTG-ase/Gdn-HCl 4.0 M	—	—	—	—	FZJ

R_g represents the gyration radius, dΣ/dΩ(0) the forward cross sections, calculated by the Guinier approximation. The number of scattering particles per unit volume, N, was calculated using Eq. 6. The nominal number of proteins per unit volume was 3.9×10^{16} cm^{-3} and 1.5×10^{16} cm^{-3} in HMI and FZJ experiments, respectively; the difference between the nominal and the experimental concentrations is also shown. In the last column, the instrument used is indicated. For the last two samples, the absence of any SANS signal in the investigated region, probably due to protein denaturation, was detected.

TABLE 2 SAXS experimental results

	R_g (Å)
nTG-ase	31.4 ± 4.2
nTG-ase/Ca^{2+}	38.6 ± 3.4
pTG-ase	31.8 ± 3.2
pTG-ase/GTP	30.1 ± 3.2
pTG-ase/Gdn-HCl (0.5 M)	30.5 ± 3.3
pTG-ase/Gdn-HCl (0.8 M)	31.2 ± 3.0
pTG-ase/Gdn-HCl (1.0 M)	19.0 ± 5.6
pTG-ase/Gdn-HCl (2.0 M)	—

R_g represents the gyration radius. For the last sample, the absence of a SAXS signal in the investigated region, probably due to protein denaturation, was detected.

presence of both Ca^{2+} and GTP, only data sets obtained at HMI and FZJ were available, respectively.

In the case of the nTG-ase, because the SAS data indicate a particle with a radius of gyration larger than the one calculated from the crystallographic structure, and because the magnitude of the effect is the same for x-rays and neutrons, the scattering intensity was calculated from the atomic model, taking into account the presence of a border shell attributed to the mobility of the protein surface (Svergun et al., 1998). According to Eq. 9, only one free parameter was adjusted in the fitting procedure, the width of the Gaussian (σ) used to describe the particle at the border (Svergun, 1997). The good fit shown in Fig. 3 and Table 3 was obtained with $\sigma = 4.40 \pm 0.05$ Å. The resulting χ^2 was 1.02.

To fit the experimental scattering data observed in the presence of GTP, Ca^{2+}, and both GTP and Ca^{2+}, we simulate the scattering volume of TG-ase by moving different regions of the protein from the position occupied in the computer-designed model. However, to reduce the number of possibilities, two relevant results were considered.

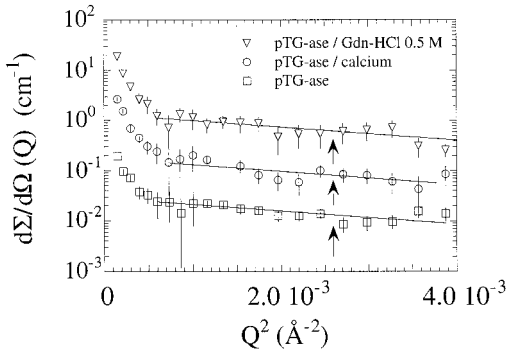

FIGURE 5 Guinier plots of SANS data obtained at FZJ for proteolyzed TG-ase dissolved in D_2O buffer without ligands (□), with 1.8 mM $CaCl_2$ (○, scaled by 10), and with 0.5 M guanidine-HCl (▽, scaled by 10^2). The solid lines correspond to the fits by the Guinier law. As reported in the text, we assumed that the contribution of the low Q^2 signal is negligible at the highest Q^2 values. The maximum Q^2 values used for the fits are indicated by arrows.

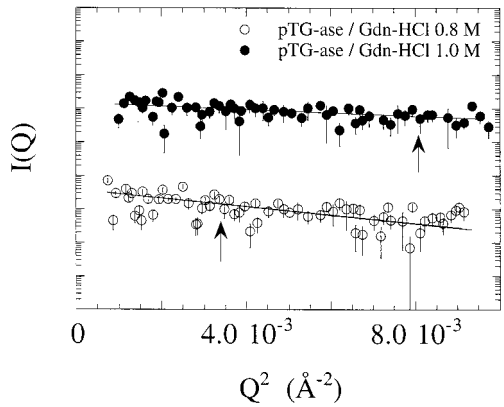

FIGURE 6 Guinier plots of SAXS data for the proteolyzed TG-ase dissolved in H_2O buffer with 0.8 M guanidine-HCl (○) and 1 M (●). The solid lines correspond to the fits by the Guinier law. As reported in the text, we assumed that the contribution of the low Q^2 signal is negligible at the highest Q^2 values. The maximum Q^2 values used for the fits are indicated by arrows.

First, 50-ps protein dynamics realized in the presence of Ca^{2+} showed that after activation the p31 peptide moves away from the p56 peptide (Casadio et al., 1999). Second, the present SAS data indicate that the cleavage of the peptide chain at the exposed loop interferes with the conformational changes.

Therefore, we analyzed all possible conformations obtained by rotating around the flexible loop and in all directions the peptide p31. In practice, according to the intrinsically low resolution of SANS experiments, the peptides were considered to be rigid. Moreover, one amino acid residue, Ala^{466}, was used as a hinge. To fit the experimental scattering curve, we also take into account the presence of the border shell attributed to the mobility of the protein surface, as determined for the native protein. Hence, the free parameters in the protein model were only the three Euler angles Ω_2, which describe the position of the p31 peptide with respect to p56.

To obtain a more accessible parameter to describe the protein conformation, we resort to the angle ψ between the longest axes of the p31 and p56 peptides. The longest axis versors $\hat{\mathbf{z}}_i$ of the ith peptide are determined by finding the reference frame in which the tensor of the inertia momentum is diagonalized. The axis $\hat{\mathbf{z}}_i$ is the one corresponding to the lowest component of the tensor. The angle ψ is easily calculated from the scalar product $\hat{\mathbf{z}}_1 \cdot \hat{\mathbf{z}}_2$. In the computer-designed model, the ψ angle is found to be 34.6°.

The Euler angles have been sampled using 20,000 points and a Monte Carlo method in the three-dimensional space α, cos β, γ. According to the standard numerical methods (Press et al., 1992), a solution (i.e., a set of angles Ω_2) is considered to be acceptable when the corresponding χ^2 is lower than 2. Solutions with a superposition volume between the two shape functions $\mathcal{F}_1(\omega_r)$ and $\mathcal{F}_2(\omega_r)$ (Fig. 2)

TABLE 3 Results of the analysis of SANS data by the Monte Carlo method described in the text

	σ (Å)	Ω_2 (°)	ψ (°)	χ^2	κ (cm^{-1})	B (cm^{-1})
nTG-ase	4.40	**(0, 0, 0)**	34.6	1.02	0.212	0.0448
nTG-ase/GTP	**4.40**	(267, 13, 107)	20	0.82	0.196	0.0429
nTG-ase/Ca^{2+}	**4.40**	(245, 29, 69)	64	1.61	0.258	0.0456
nTG-ase/GTP/Ca^{2+}	**4.40**	(245, 29, 69)	64	0.78	0.258	0.0456

σ is the width of the Gaussian that accounts for the particle surface mobility; Ω_2 are the three Euler angles that describe the position of the p31 peptide with respect to p56; χ^2 is the reduced chi squared (see Eq. 11); κ is a scaling factor; B is a flat background. The fixed parameters are in bold. Apart from the first case, the fitting parameters refer to one of the possible solutions shown in Fig. 3.

greater than a threshold value of 5000 $Å^3$ were not considered. The final result is then described by the histogram $\mathcal{H}(\psi, \chi^2 \leq 2)$ (Fig. 7), giving the probability of obtaining an acceptable conformation with an angle ψ.

To check the sensitivity of the method, we first reanalyzed the data obtained from the pure nTG-ase fixing σ = 4.40 Å and sampling the Ω_2 angle set. The resulting histogram, shown in Fig. 7, presents a maximum around ψ =

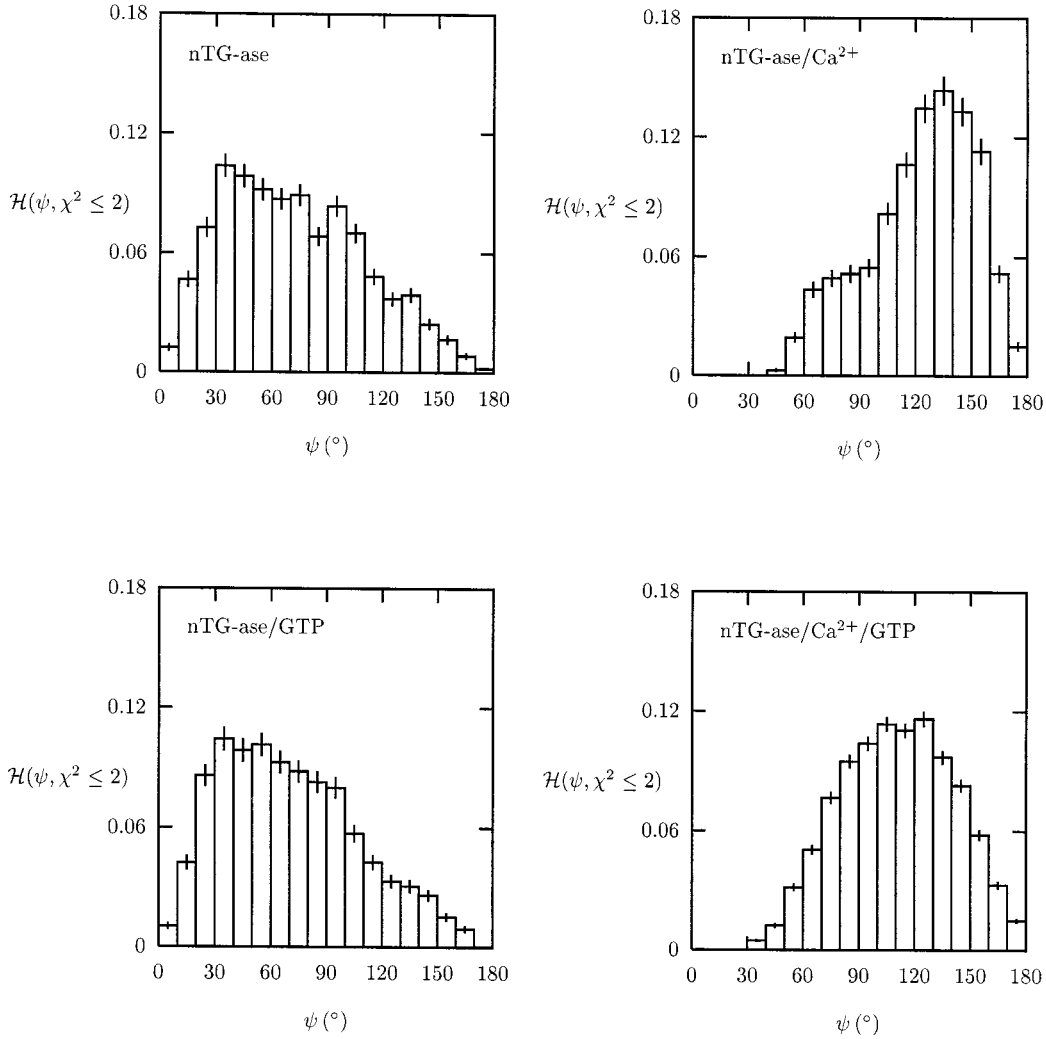

FIGURE 7 Probability histograms of the TG-ase conformational angle ψ obtained from the Monte Carlo analysis of the SANS data (ψ is the angle between the longest axes of the two peptides p31 and p56). The histograms were calculated by sampling the Euler angle space Ω_2 and considering as acceptable only conformations giving a goodness of fit of $\chi^2 \leq 2$. The different experimental conditions are indicated in the frames.

35°. However (in connection with the low resolution of the scattering data), all of the other conformations appear to be populated as well.

In the case of the nTG-ase/GTP sample, the histogram (again see Fig. 7) is rather similar to the one obtained for the pure nTG-ase, but a significative difference appears in the increasing population of conformations with ψ lower than 30°. As an example, the fitting curve relative to one of these solutions (see Table 3) is reported in Fig. 3, and a view of the corresponding TG-ase conformation appears in Fig. 8.

For the Ca^{2+}-activated structure and the TG-ase sample containing both Ca^{2+} and GTP, the histograms show a clear shift toward larger ψ angles (see Fig. 7). In particular, conformations with ψ lower than 50° are not compatible with the experimental data. Even if both histograms show a maximum at ~130°, to show the smallest difference with the native conformation, we describe one of the solutions belonging to the first significatively populated bin (ψ = 60 ÷ 70°). In Fig. 8 the protein conformation with $\psi = 64°$ is shown: the corresponding fitting parameters are reported in Table 3 and the fitting curves appear in Fig. 3.

DISCUSSION

The increasing biological and biophysical interest in transglutaminases (Aeschlimann et al., 1995) explains the relevance of structural studies devoted to clarifying the basis of regulation of the protein activity. The scattering data presented here highlight the characteristics of conformational changes promoted by negative and positive effectors, i.e., GTP and Ca^{2+}. The structure of the native TG-ase has recently been modeled by homology building (Casadio et al., 1999). The wide prolate ellipsoidal shape of the protein is shown in Fig. 1; the present neutron and x-ray small-angle scattering data are fully compatible with this structural model. By Monte Carlo simulation of the scattering of the protein, a perfect agreement with the SANS experimental curve is obtained by using the modeled structure and taking into account a border shell attributed to the mobility of the protein surface. The presence of this shell is consistent with the increase in the apparent size of proteins in solution detected by both SANS and SAXS experiments (Svergun, 1997).

Concerning the ligand effects, a small but significant decrease in the gyration radius was observed after saturation with GTP. On the other hand, large differences in the scattering profile, indicating a widening of the structure, were detected after Ca^{2+} addition, both with and without GTP. Because the analysis of the forward neutron scattering indicates that these modifications cannot be ascribed to protein aggregation processes (like dimerization), SAS results demonstrate that conformational changes are promoted by ligand binding. In agreement with previous kinetic studies (Bergamini, 1988), the present work also confirms the predominant role of Ca^{2+} in dictating the final conformational state (and hence the functional state) of TG-ase.

Although the proteolyzed enzyme was observed to significantly aggregate in heavy water, two results should be noticed. First, SAS data indicate that after proteolysis the two peptides are mostly joined by intermolecular interactions. However, guanidine is expected to interfere with forces at the interface between the two peptides. Accordingly, at the appropriate Gdn-HCl concentration, the presence of smaller scattering particles was observed. Inside the experimental uncertainty, the measured radius of gyration corresponds to the value calculated for the p31 peptide; although the resolution of the SAXS experiments is not enough to exclude the presence of the p56 peptide, this observation might indicate that the N-terminal p56 peptide

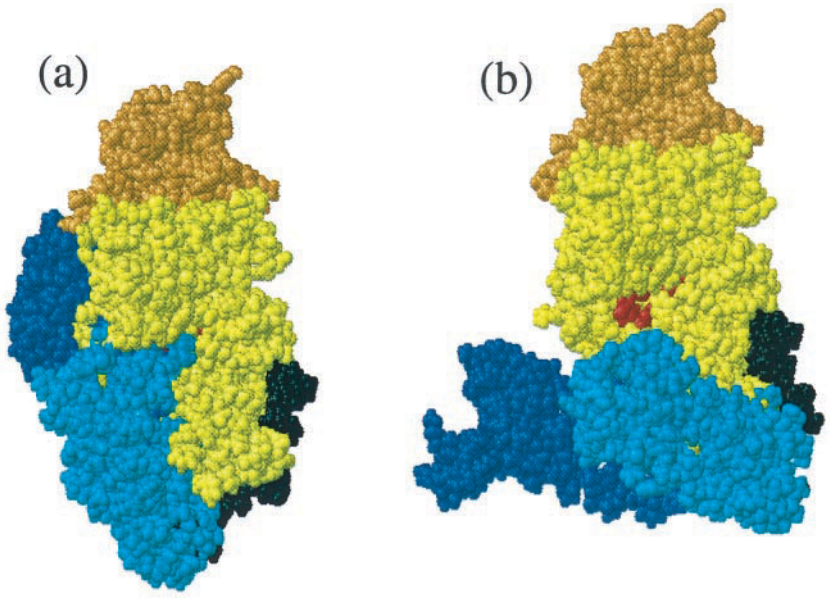

FIGURE 8 Three-dimensional representation of possible structures of TG-ase with GTP and with Ca^{2+}, reconstructed from SANS profiles by a Monte Carlo method and starting from the computer-designed model and molecular dynamics results. (*a*) Conformation representative of TG-ase with GTP. The p31 peptide is rigidly rotated around Ala^{466} by the Euler angles of 267°, 13°, and 107° with respect to the p56 peptide. The corresponding ψ angle between the longest axes of the two peptides is 20°. (*b*) Conformation representative of TG-ase with either Ca^{2+} or Ca^{2+}/GTP. The p31 peptide is rigidly rotated around Ala^{466}, using Euler angles of 245°, 29°, and 69° with respect to the p56 peptide. The corresponding ψ angle between the longest axes of the two peptides is 64°. Notice that in both views, the four domains are represented by the colors used in Fig. 1 and that the p56 peptide displays the same orientation showed in that figure. Note also that the high resolution of the structural representation is not derived from SANS data, which only allows the motions of specific peptides to be addressed.

plays an important role in the denaturation and in the extended aggregation (C. M. Bergamini, unpublished observations). The second point is relevant for the protein structural changes: after proteolysis the Ca^{2+}-dependent widening of TG-ase is no longer observed. The cleavage of the peptide chain at the exposed loop interferes with the hinge function.

By combining these observations with protein dynamics simulations realized in the presence of Ca^{2+} (Casadio et al., 1999), a rough model for TG-ase structure after ligand binding was built. In particular, we assumed that the observed conformational changes concern only the arrangement of the p31 peptide, which is moved from the position occupied on the computer-designed model by rotating around the flexible loop. Because the structure of the protein in the native state is available, the possible conformations available for the protein with the ligand were then reconstructed by fitting the experimental SANS curves, using the Monte Carlo simulation of the scattering described above.

The Monte Carlo analysis shows that in the presence of Ca^{2+} and in the presence of both Ca^{2+} and GTP, the minimum angle ψ between the p56 and p31 peptides is 50°, larger than the one observed in the native conformation (34.6°). As an example, in Fig. 8 is shown the conformation with $\psi = 64°$. The widening of the cleft that makes the active site available can be clearly appreciated. It should be noticed that this conformation is already sufficient to accommodate macromolecular substrates—conformations with larger ψ are more and more favorable.

With respect to the structure of native TG-ase, the Monte Carlo simulation of the protein shape in the presence of GTP indicates that the contact between the p31 and p56 peptides can be even closer, i.e., the population of conformations with ψ lower than 30° increases. This effect can be appreciated by comparing the models shown in Fig. 8. After GTP binding, peptide p31 appears to embrace more closely peptide p56; the resulting catalytic triad is shielded from contact with the solvent or with protein substrates, with the inhibition of enzyme activity. It is noticeable that these results confirm recent conclusions obtained by immunoreactions with antibodies and site-directed mutagenesis (Monsonego et al., 1997). In particular, our data support the idea that the role of GTP in TG-ase activity is also related to the integrity of the C-terminal region. According to the deduced conformational change, any modification in the C-terminal sequence might also result in structural and functional differences that would affect the GTP binding.

Because the mechanics of the model used in the fitting procedures is simple and the possible movements of the peptides are bounded by severe assumptions, these results have to be considered as a simplification of the real conformational changes. However, the reconstructed structural models agree completely with previous fluorescence and IR spectroscopy measurements and with the differences observed in biochemical reactivity (Tanfani et al., 1993; Bergamini, 1988; Bergamini and Signorini, 1993; Monsonego et al., 1997, 1998). In the absence of the crystallographic structure of the ligand stabilized conformations, SAS experiments are then successful for a direct monitoring of TG-ase structural properties. Moreover, because a high-resolution structure is available, the Monte Carlo procedure described here is a powerful technique for obtaining a low-resolution description of protein structural changes after activation or inhibition by ligands. The biological meaning of the results is straightforward: according to the TG-ase bifunctional activity and to the fact that the cross-linking activity of TG-ase is latent in cycling cells through the combined action of two effectors, Ca^{2+} and GTP, it is clearly demonstrated that control is achieved through massive conformational changes.

We are grateful to Prof. F. Rustichelli for helpful suggestions and discussion.

This work was partially financed by the Ministero dell'Università e della Ricerca Scientifica e Tecnologica (MURST) (Italy). RC was supported partially by a grant for a target project in Biotechnology from Consiglio Nazionale delle Ricerche (Italy) and by a grant to the project "Biocatalisi e Bioconversioni" from MURST (Italy).

REFERENCES

Aeschlimann, D., O. Kaupp, and M. Paulsson. 1995. Transglutaminase-catalyzed matrix cross-linking in differentiating cartilage: identification of ostenonectin as major glutaminyl substrate. *J. Cell. Biol.* 129: 881–889.

Ashton, A. W., M. K. Boehm, J. R. Gallimore, M. B. Pepys, and S. J. Perkins. 1997. Pentameric and decameric structures in solution of serum amyloid P component by x-ray and neutron scattering and molecular modelling analyses. *J. Mol. Biol.* 272:408–422.

Bergamini, C. M. 1988. GTP modulates Ca^{2+} binding and cation-induced conformational changes in erythrocyte transglutaminase. *FEBS Lett.* 239:255–258.

Bergamini, C. M., and M. Signorini. 1993. Studies on tissue transglutaminases. Interaction on erythrocyte type 2 transglutaminase with GTP. *Biochem. J.* 291:37–39.

Casadio, R., E. Polverini, P. Mariani, F. Spinozzi, F. Carsughi, A. Fontana, P. Polverino de Laureto, G. Matteucci, and C. M. Bergamini. 1999. The structural basis for the regulation of tissue transglutaminase by calcium ions. *Eur. J. Biochem.* 262:672–679.

Chacon, P., F. Moran, J. F. Diaz, E. Pantos, and J. M. Andreu. 1998. Low resolution structures of proteins in solution retrieved from x-ray scattering with a genetic algorithm. *Biophys. J.* 74:2760–2775.

Chen, S. H., and D. Bendedouch. 1986. Structure and interactions of proteins in solution studied by small angle neutron scattering. *Methods Enzymol.* 130:79–116.

Eliezer, D., P. Frank, N. Gills, W. E. Newton, S. Doniach, and K. O. Hodgson. 1993. Small-angle x-ray scattering studies of the iron-molybdenum cofactor from *Azotobacter vinelandii* nitrogenase. *J. Biol. Chem.* 268:20953–20957.

Fesus, L., P. J. A. Davies, and M. Piacentini. 1991. Apoptosis: molecular mechanisms in programmed cell death. *Eur. J. Cell. Biol.* 56:170–177.

Folk, J. E., and J. S. Finnlayson. 1977. The ϵ-(γ-glutamyl)lysine cross-link and the catalytic activity of transglutaminases. *Adv. Protein Chem.* 31:1–133.

Glatter, O., and O. Kratky. 1982. Small angle x-ray scattering. Academic Press, New York.

Greenberg, C. S., P. J. Birckbichler, and R. H. Rice. 1991. Transglutaminases: multifunctional cross-linking enzymes that stabilize tissues. *FASEB J.* 5:3071–3077.

Guinier, A., and G. Fournet. 1955. Small Angle Scattering of X-Ray. Wiley, New York.

Hansen, S. 1990. Calculation of small-angle scattering profiles using Monte Carlo simulation. *J. Appl. Crystallogr.* 23:344–346.

Henderson, S. J. 1996. Monte Carlo modeling of small-angle scattering data from noninteracting homogeneous and heterogeneous particles in solution. *Biophys. J.* 70:1618–1627.

Jacrot, B. 1976. The study of biological structures by neutron scattering from solution. *Rep. Prog. Phys.* 39:911–953.

Jacrot, B., and G. Zaccai. 1981. Determination of molecular weight by neutron scattering. *Biopolymers.* 20:2413–2426.

Kataoka, M., I. Nishii, I. Fujisawa, T. Ueki, T. Tokunaga, and Y. Goto. 1995. Structural characterization of the molten globule and native states of apomyoglobin by solution x-ray scattering. *J. Mol. Biol.* 249: 215–228.

Mayans, M. O., W. J. Coadwell, D. Beale, D. B. A. Symons, and S. J. Perkins. 1995. Demonstration by pulsed neutron scattering that the arrangement of Fab and Fc fragments in the overall structures of bovine IgG_1 and IgG_2 in solution is similar. *Biochem. J.* 311:282–291.

Mian, S., S. el Alaoui, J. Lawry, V. Gentile, P. J. Davies, and M. Griffin. 1995. The importance of the GTP-binding protein tissue transglutaminase in the regulation of cell cycle progression. *FEBS Lett.* 370:27–31.

Monsonego, A., I. Friedmann, Y. Shani, M. Eisenstein, and M. Schwartz. 1998. GTP-dependent conformational changes associated with the functional switch between Gα and cross-linking activities in brain-derived tissue transglutaminase. *J. Mol. Biol.* 282:713–720.

Monsonego, A., Y. Shani, I. Friedmann, Y. Paas, O. Eizenberg, and M. Schwartz. 1997. Expression of GTP-dependent and GTP-independent tissue-type transglutaminase in cytokine-treated rat brain astrocytes. *J. Biol. Chem.* 272:3724–3732.

Muller, K., and O. Glatter. 1982. Practical aspects to the use of indirect Fourier transformation methods. *Makromol. Chem.* 183:465–479.

Nakanishi, K., K. Nara, H. Hagiwara, Y. Aoyama, H. Ueno, and S. Hirose. 1991. Cloning and sequence analysis of cDNA clones for bovine aortic endothelial cell transglutaminases. *Eur. J. Biochem.* 202:15–21.

Nakaoka, H., D. M. Perez, K. J. Baek, T. Das, A. Husain, K. Misono, M. J. Im, and R. M. Graham. 1994. G_h: a GTP binding protein with transglutaminase activity and receptor signalling function. *Science*. 264: 1593–1596.

Pedersen, L. C., V. C. Yee, P. D. Bishop, L. I. Trong, D. C. Teller, and R. E. Stenkamp. 1994. Transglutaminase factor XIII uses proteinase-like catalytic triad to cross-link macromolecules. *Protein Sci.* 3:1131–1135.

Press, W. H., S. A. Teukolsky, W. T. Vetterling, and B. P. Flannery. 1992. Numerical Recipes. Cambridge University Press, Cambridge, UK.

Shi, L., M. Kataoka, and A. L. Fink. 1996. Conformational characterization of DnaK and its complexes by small-angle x-ray scattering. *Biochemistry.* 35:3297–3308.

Siefring, G. E., A. B. Apostol, P. T. Velasco, and L. Lorand. 1978. Enzymatic basis for the Ca^{2+}-induced cross-linking of membrane proteins in intact human erythrocytes. *Biochemistry.* 17:2598–2604.

Smethurst, P. A., and M. Griffin. 1996. Measurement of tissue transglutaminase activity in a permeabilized cell system: its regulation by Ca^{2+} and nucleotides. *Biochem. J.* 313:803–808.

Spinozzi, F., F. Carsughi, and P. Mariani. 1998. Particle shape reconstruction by small-angle scattering. Integration of group theory and maximum entropy to multipole expansion method. *J. Chem. Phys.* 109: 10148–10158.

Svergun, D. I. 1991. Mathematical methods in small-angle scattering data analysis. *J. Appl. Crystallogr.* 24:485–492.

Svergun, D. I. 1997. Restoring three-dimensional structure of biopolymers from solution scattering. *J. Appl. Crystallogr.* 30:792–797.

Svergun, I., S. Richard, M. H. J. Koch, Z. Sayers, S. Kuprin, and G. Zaccai. 1998. Protein hydration in solution: experimental observation by x-ray and neutron scattering. *Proc. Natl. Acad. Sci. USA.* 95:2267–2272.

Svergun, D. I., and H. B. Stuhrman. 1991. New developments in direct determination from small-angle scattering. 1. Theory and model calculations. *Acta Crystallogr. A.* 47:736–744.

Tanfani, F., E. Bertoli, M. Signorini, and C. M. Bergamini. 1993. Structural investigation of transglutaminase by Fourier transform infrared spectroscopy. *Eur. J. Biochem.* 218:499–505.

Trewhella, J. 1997. Insights into biomolecular function from small-angle scattering. *Curr. Opin. Struct. Biol.* 7:702–708.

Zhang, J., M. Lesort, R. P. Guttmann, and G. V. Johnson. 1998. Modulation of the in situ activity of tissue transglutaminase by calcium and GTP. *J. Biol. Chem.* 273:2288–2295.